

Revised phase diagram of a high- T_c cuprate superconductor revealed by anisotropic transport measurements

Keiichi Harada,¹ Yuki Teramoto,¹ Tomohiro Usui,¹ Kenji Itaka,² Takenori Fujii,³ Takashi Noji,⁴ Haruka Taniguchi,⁵ Michiaki Matsukawa,⁵ Hajime Ishikawa,⁶ Koichi Kindo,⁶ Daniel S. Dessau,⁷ and Takao Watanabe^{1,*}

¹Graduate School of Science and Technology, Hirosaki University, Hirosaki, Aomori, 036-8561 Japan

²Institute of Regional Innovation, Hirosaki University, Aomori, Aomori, 036-8561 Japan

³Cryogenic Research Center, University of Tokyo, Bunkyo, Tokyo 113-0032, Japan

⁴Graduate School of Engineering, Tohoku University, Sendai 980-8579, Japan

⁵Graduate School of Engineering, Iwate University, Morioka 020-8551, Japan

⁶Institute for Solid State Physics, University of Tokyo, Kashiwa, Chiba 277-8581, Japan

⁷Department of Physics, University of Colorado at Boulder, Boulder, CO 80309, USA

(Dated: February 28, 2022)

The phase diagram of high transition temperature (high- T_c) cuprates is elucidated via systematic anisotropic transport measurements for Pb-doped Bi-2212 single crystals. We demonstrate that the onset temperatures of the “weak” pseudogap and electronic coherence cross each other at a critical doping level, while the onset of the “strong” pseudogap merges into that of superconducting fluctuations above the critical doping level. These results indicate the importance of Mottness in high- T_c superconductivity.

Introduction.—Superconductivity is an instability of the normal metallic state. Therefore, to understand the mechanism of superconductivity, it is important to understand the normal state from which superconductivity emerges [1]. The features of the normal state can be evaluated from the doping per Cu (p)-temperature (T) phase diagram. Two types of theoretical phase diagrams have been proposed for cuprates. The first is the quantum critical point (QCP) model [2, 3], in which T^* (onset temperatures of the pseudogap) and T_{coh} (crossover temperatures from the metal state at higher temperatures to the Fermi-liquid state at lower temperatures) vanish at the QCP (Fig. 1(a)). The fluctuations associated with the quantum critical phase transition mediate the Cooper pairing. The second is the resonating valence bond (RVB) model [4–6]. Here, we evaluate the RVB model that considers the fluctuations of the gauge fields to which spinons and holons are strongly coupled, since those fluctuations play an important role in the charge dynamics, such as transport properties [4–6]. In this model, T_D (spin gap opening temperatures or its mean-field solution, $T_D^{(0)}$) and T_{BE} (temperatures for the Bose condensation of holons or its mean-field solution, $T_{BE}^{(0)}$) which corresponds to T_{coh} , cross each other at a finite temperature near optimal doping (Fig. 1(b)). Here, large spin correlations arising from the Mottness serve as the source for Cooper pairing. However, the level of accuracy of these two phase diagrams has been debated upon in literature [7].

The positional relationship between the pseudogap (or spin gap) opening temperatures and T_{coh} is unclear. In contrast to the pseudogap [1, 8–11], the behavior of T_{coh} has rarely been reported [12–15], and a general consensus has not been obtained yet [7]. This can be attributed to the limited number of materials that can be examined. Pb-doped Bi-2212 is a suitable choice for such an investigation, because the doping levels can be controlled from the nearly optimal value to beyond the critical doping level $p = 0.19$ via oxygen annealing [16, 17].

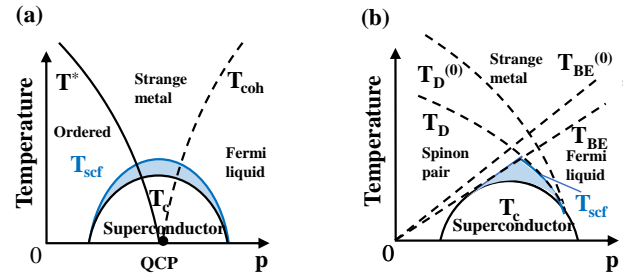


FIG. 1. (Color online) Schematic phase diagrams for (a) a QCP model [2, 3] and (b) a RVB model that considers the gauge field fluctuations [4–6]. In each figure, the black bold lines denote the true phase transition temperatures, whereas the black dashed lines denote the crossover temperatures. The blue shaded area denotes the superconducting fluctuation regime. Here, the original phase transition temperatures of the RVB model are represented by T_{scf} , considering the strong two-dimensionality of cuprates.

Here, we first measured the anisotropic transport properties of Bi(Pb)-2212, and estimated the characteristic temperatures at which the typical temperature evolution occurs. Then, we drew a true electronic phase diagram of Bi(Pb)-2212, which shows that i) two types (“weak” and “strong”) of pseudogaps exist, ii) they terminate at different p ’s, and iii) the onset temperatures of the “weak” pseudogap and T_{coh} intersect. Finally, we discuss the implications of the obtained phase diagram.

Methods.—Single crystals of $\text{Bi}_{1.6}\text{Pb}_{0.4}\text{Sr}_2\text{CaCu}_2\text{O}_{8+\delta}$ (nominal composition of $\text{Bi}_{1.6}\text{Pb}_{0.6}\text{Sr}_2\text{CaCu}_2\text{O}_{8+\delta}$) were grown in air using the traveling solvent floating zone method. The crystals were annealed by varying the oxygen partial pressure, P_{O_2} , ($2 \text{ Pa} \leq P_{O_2} \leq 400 \text{ atm}$), at 400–600 °C for sufficient durations to homogeneously control the corresponding doping levels for sample preparation (see Supplemental Materials [19]). Moreover, previously reported data for excessively overdoped ($p = 0.232$) pristine samples [18] were included in the

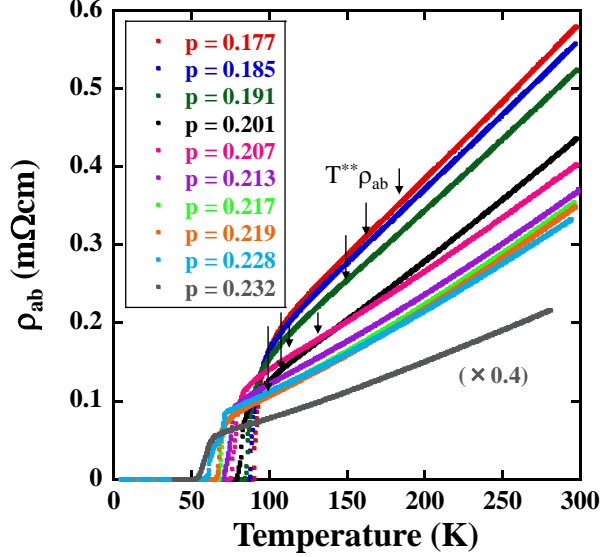


FIG. 2. (Color online) In-plane resistivity $\rho_{ab}(T)$ for $\text{Bi}_{1.6}\text{Pb}_{0.4}\text{Sr}_2\text{CaCu}_2\text{O}_{8+\delta}$ single crystals with various p . The most overdoped sample with $p = 0.232$ is pristine $\text{Bi}_2\text{Sr}_2\text{CaCu}_2\text{O}_{8+\delta}$ [18]. The temperatures $T_{\rho_{ab}}^*$ below which $\rho_{ab}(T)$ decreases rapidly are indicated by arrows.

analysis, and we determined T_c at the onset of zero resistivity. The doping level (p) was obtained using the empirical relation [20], with maximum $T_c = 91.7$ K and 91.0 K for Pb-doped single crystals and pristine samples, respectively.

$\rho_{ab}(T)$ and $\rho_c(T)$ were measured using the DC four-terminal method. In addition, to estimate the onset temperatures for the superconducting fluctuation, T_{scf} , $\rho_{ab}(T)$ was measured using a physical property measurement system (Quantum Design) with and without a magnetic field of 9 T parallel to the c -axis.

Results.—Figure 2 shows the temperature dependence of $\rho_{ab}(T)$ for $\text{Bi}_{1.6}\text{Pb}_{0.4}\text{Sr}_2\text{CaCu}_2\text{O}_{8+\delta}$ single crystals with various p . T_c decreases systematically from 89.3 K to 65.0 K (52.0 K for the pristine sample) with increasing oxygen content, indicating that the measured samples are in the overdoped region. In the slightly overdoped region ($0.175 \leq p \leq 0.191$), $\rho_{ab}(T)$ is approximately linear in T , which is consistent with a previous report [21]. However, with further increasing doping level, $\rho_{ab}(T)$ exhibits a typical upward curvature.

To investigate the temperature dependence of $\rho_{ab}(T)$ in detail, the derivative with respect to temperature for several values of p is plotted as a function of the temperature in Fig. 3 (a). At higher temperatures, the derivative is approximately linear in T , whereas below the temperature region 180–100 K, it exhibits a steep upward curvature, reflecting the steep decrease in $\rho_{ab}(T)$ upon cooling. Here, we define the characteristic temperature at which the temperature derivative of

$\rho_{ab}(T)$ is minimized as $T_{\rho_{ab}}^*$. $T_{\rho_{ab}}^*$ is estimated as 160, 150, 130, and 102 K for $p = 0.185, 0.191, 0.201$, and 0.219, respectively. $T_{\rho_{ab}}^*$ may correspond to $T_{\rho_{ab}}^*$ which was previously defined for the underdoped Bi-2212 [18, 21].

The high-temperature T -linear behavior of the temperature derivative of $\rho_{ab}(T)$ indicates that $\rho_{ab}(T)$ can be expressed as [13, 22],

$$\rho_{ab}(T) = \alpha_0 + \alpha_1 T + \alpha_2 T^2, \quad (1)$$

where α_0 is the residual resistivity, α_1 is the coefficient of the non-Fermi-liquid T -linear term, and α_2 is the coefficient of the Fermi-liquid T^2 term. The slope and y-intercept of $d\rho_{ab}/dT$ represent $2\alpha_2$ and α_1 , respectively. However, a closer look at the data reveals that the slope below 200 K is slightly larger than that above 200 K. Thus, the coefficients are obtained below and above 200 K separately by the linear fits (Fig. 3 (a)), and are denoted as $\alpha_1(0)$, $\alpha_2(0)$, and $\alpha_1(\infty)$, $\alpha_2(\infty)$, respectively. The rise (fall) in $\alpha_2(\alpha_1)$ upon cooling implies that the electronic state approximates that of the Fermi liquids in the lower temperature region. On this basis, T_{coh} is defined by the temperature at which both linearly fitted lines intersect. As expected, T_{coh} is estimated to be approximately 200 K for all doping levels (Fig. 3 (a)).

Figures 3(b) and 3 (c) depict the doping dependence of α_1 and α_2 , respectively. With increasing doping above 0.19, $\alpha_1(\alpha_2)$ decreases (increases), implying that the system acquires a Fermi-liquid-like nature in this doping range. This result is consistent with recent angle-resolved photoemission spectroscopy (ARPES) measurements of Pb-doped Bi-2212, which reveal that with increasing doping across $p = 0.19$, the incoherent spectral function abruptly reconstructs into a coherent one near the Brillouin zone boundary [17]. The decrease in $\alpha_1(0)$ for $p > 0.19$ is consistent with previous reports for $\text{La}_{2-x}\text{Sr}_x\text{CuO}_4$ (LSCO) [13, 22] and $\text{Tl}_2\text{Ba}_2\text{CuO}_{6+\delta}$ (Tl-2201) [14]. However, with a further increase in doping, α_2 exhibits a peak at approximately $p = 0.22$. This may be related to the reported Lifshitz transition at $p = 0.22$, where the Fermi surface originating from the antibonding states changes its topology from an open hole-like state to a closed electron-like state [23, 24]. The van Hove singularity then crosses the Fermi level, which causes a peak in γ . The observed peak in α_2 may be attributed to the empirical fact that the Kadowaki-Woods ratio, α_2/γ^2 , is maintained constant within the same series of compounds [25, 26]. In addition, we find that the difference between $\alpha_1(0)(\alpha_2(0))$ and $\alpha_1(\infty)(\alpha_2(\infty))$ is expanded continuously for $p \geq 0.19$. This implies that the system becomes more Fermi-liquid-like below T_{coh} with an increasing doping level.

Figure 4(a) shows the temperature dependence of the out-of-plane resistivity, $\rho_c(T)$ for $\text{Bi}_{1.6}\text{Pb}_{0.4}\text{Sr}_2\text{CaCu}_2\text{O}_{8+\delta}$ single crystals with various p . The most overdoped sample ($p = 0.232$) is pristine $\text{Bi}_2\text{Sr}_2\text{CaCu}_2\text{O}_{8+\delta}$. Although $\rho_c(T)$ exhibits metallic behavior above 250 K, the gradual upturn below a certain temperature $T_{\rho_c}^*$ is an indication of the opening of the

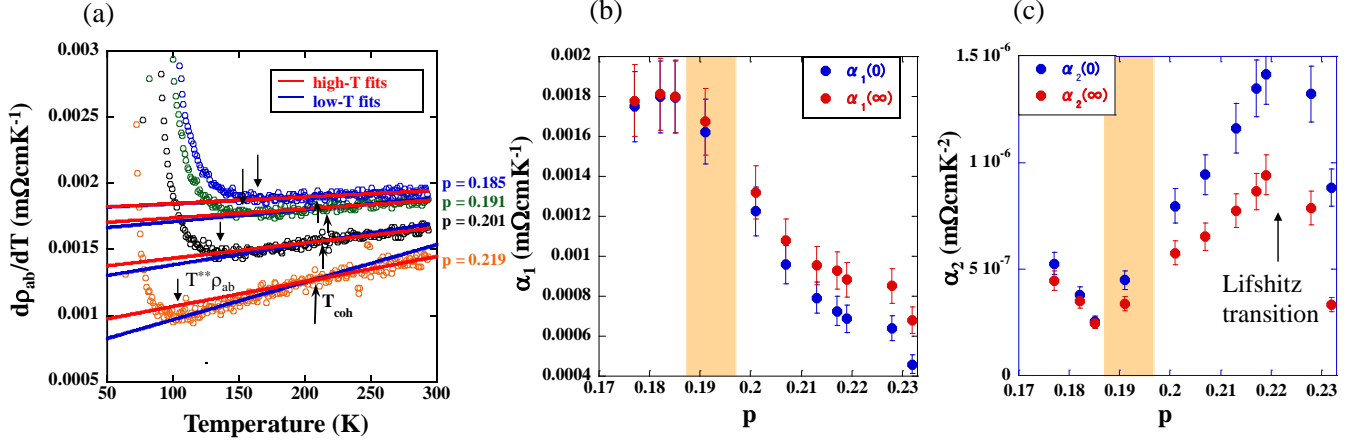


FIG. 3. (Color online) (a) Temperature derivative of ρ_{ab} vs. temperature for several p . The temperatures $T_{\rho_{ab}}^{**}$ at which $d\rho_{ab}/dT$ is minimum and T_{coh} at which high-temperature and low-temperature linear fits intersect are indicated by arrows. (b) The coefficient of the T -linear term in $\rho_{ab}(T)$, α_1 , vs. p . $\alpha_1(\infty)$ and $\alpha_1(0)$ is obtained by the linear fits for $d\rho_{ab}/dT$ at high and low temperatures, respectively. (c) The coefficient of the T^2 term in $\rho_{ab}(T)$, α_2 , vs. p . $\alpha_2(\infty)$ and $\alpha_2(0)$ is obtained by the linear fits for $d\rho_{ab}/dT$ at high and low temperatures, respectively.

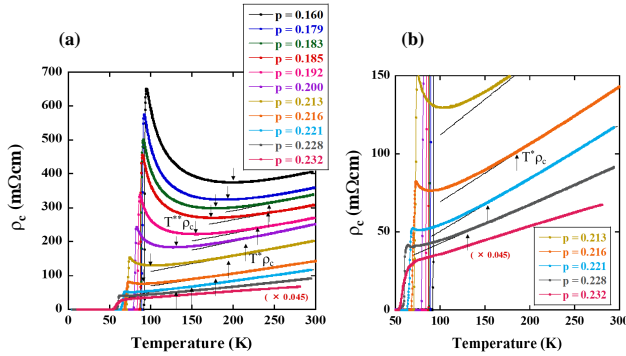


FIG. 4. (Color online) (a) Out-of-plane resistivity $\rho_c(T)$ for $\text{Bi}_{1.6}\text{Pb}_{0.4}\text{Sr}_2\text{CaCu}_2\text{O}_{8+\delta}$ single crystals with various p . The most overdoped sample with $p = 0.232$ is pristine $\text{Bi}_2\text{Sr}_2\text{CaCu}_2\text{O}_{8+\delta}$ [18]. The temperatures $T_{\rho_c}^*$ below which $\rho_c(T)$ gradually increases and $T_{\rho_c}^{**}$ at which $\rho_c(T)$ is minimized are indicated by arrows. (b) Expanded view of the overdoped side of (a).

pseudogap [18, 21, 27] (hereafter referred to as “weak” pseudogap [1]). $T_{\rho_c}^*$ is determined using a previously reported definition [18, 21, 27]. $T_{\rho_c}^*$ is high even for $p > 0.19$, but decreases rapidly when p exceeds 0.22. However, $T_{\rho_c}^*$ cannot be determined above T_c at $p = 0.232$ (Fig. 4(b)). At temperatures below $T_{\rho_c}^*$, $\rho_c(T)$ increases rapidly below $T_{\rho_c}^{**}$. This suggests that another pseudogap (hereafter referred to as “strong” pseudogap [1]) opens up below this temperature. $T_{\rho_c}^{**}$ is estimated as 198, 189, 178, 176, 153, 129, 101, and 90 K for $p = 0.160, 0.179, 0.183, 0.185, 0.192, 0.200, 0.213$, and 0.216 , respectively. Here, $T_{\rho_c}^{**}$ is defined as the temperature at which $\rho_c(T)$ is minimized. $T_{\rho_c}^{**}$ cannot be determined for $p \geq 0.221$, because the rapid increase is not observed in these samples.

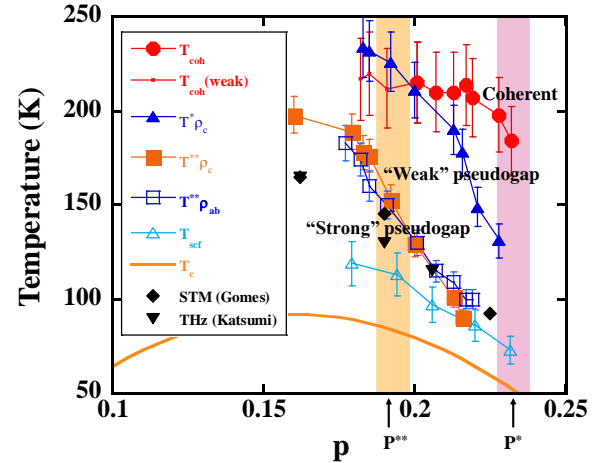


FIG. 5. (Color online) Characteristic temperatures vs. p for $\text{Bi}_{1.6}\text{Pb}_{0.4}\text{Sr}_2\text{CaCu}_2\text{O}_{8+\delta}$ and $\text{Bi}_2\text{Sr}_2\text{CaCu}_2\text{O}_{8+\delta}$ [18] single crystals. The black closed diamonds representing scanning tunneling microscopy (STM) and down-pointing triangles representing THz are adopted from Ref. [28] and Ref. [29], respectively. The orange and purple bands indicate the characteristic doping levels of $p^{**} \approx 0.19$ and $p^* \approx 0.23$, respectively.

To investigate the relationship between the “weak” and “strong” pseudogap opening temperatures and T_{scf} , T_{scf} was estimated by comparing the values of $\rho_{ab}(T)$ with and without a magnetic field. The results are consistent with those in our previous studies [18, 27] and are discussed in the Supplemental Materials [19].

Phase diagram.—The characteristic temperatures T_{coh} , $T_{\rho_c}^*$, $T_{\rho_c}^{**}$, $T_{\rho_{ab}}^{**}$, and T_{scf} are plotted as functions of p in Fig. 5.

The plots show that $T_{\rho_c}^{**}$ and $T_{\rho_{ab}}^{**}$ coincide, which indicates that both have the same origin (i.e., the onset of the “strong” pseudogap). The rapid decrease in $\rho_{ab}(T)$ below $T_{\rho_{ab}}^{**}$ may be due to the decreasing scattering rate upon opening of the “strong” pseudogap. On this basis, we denote T^{**} as representing $T_{\rho_c}^{**}$ and $T_{\rho_{ab}}^{**}$ collectively. For $p \leq 0.19$, T^{**} differs from T_{scf} , whereas for $p > 0.19$, T^{**} rapidly approaches T_{scf} , and eventually coincides with it at $p \approx 0.21$.

Next, we discuss the end point, p^* , of the “weak” pseudogap. Figure 5 shows that $T_{\rho_c}^*$ decreases rapidly for $p > 0.22$, and then disappears at $p \approx 0.23$. This result suggests that $p^* \approx 0.23$ for the Bi-2212 case. As discussed in Fig. 3(c), we observed a kink in the T^2 coefficient, α_2 , of $\rho_{ab}(T)$ at $p = 0.22$, where Lifshitz transition occurs [23]. Then, the disappearance for $T_{\rho_c}^*$ at $p \approx 0.23$ may be attributed to this Lifshitz transition, since the spectral weights at anti-nodal directions, which are needed to open the “weak” pseudogap, are expected to decrease after the transition [24].

Finally, in this section, we demonstrate the positional relationship between T_{coh} and $T_{\rho_c}^*$. Figure 5 shows that T_{coh} is independent of the doping level, with a slight tendency to decrease with excessive overdoping. Moreover, T_{coh} exists even below $p = 0.19$, although the difference in the temperature dependence of $\rho_{ab}(T)$ below and above T_{coh} is small. This may be attributed to the fact that for $p < 0.19$, the feature accompanied by electronic coherence is masked by the higher onset of the “weak” pseudogap. These results indicate that $T_{\rho_c}^*$ and T_{coh} intersect at $p = 0.19$.

Discussion.—Here, we discuss the implications of the obtained results. First, we accurately determined the onset of two types of pseudogaps ($T_{\rho_c}^*$ and T^{**} for the “weak” and “strong” pseudogaps, respectively) by combining the results of the in-plane and out-of-plane transport measurements (Fig. 5). Then, we found that T^{**} differed from T_{scf} for $p \leq 0.19$, while they coincided for $p > 0.19$. Based on this result, we considered that the “strong” pseudogap originated from the preformed Cooper pairing (phase-incoherent Cooper pair formation) in the QCP model (Fig. 1(a)) or the spinon pairing in the RVB model (Fig. 1(b)). Thus far, although several measurements have reported preformed Cooper pairings in high- T_c cuprates [28, 29, 31–39], a general consensus has not been realized [7]. Furthermore, the doping levels for which these distinct pseudogaps terminate are unknown. We found that T^{**} ends (or merges with T_{scf}) at approximately $p^* = 0.19$, whereas $T_{\rho_c}^*$ ends at approximately $p^* = 0.23$ for Pb-doped Bi-2212. Given that p^* of $\text{YBa}_2\text{Cu}_3\text{O}_{7-\delta}$ is 0.19 [40], it may be material (i.e., band structure)-dependent [24].

Next, we found that $T_{\rho_c}^*$ and T_{coh} cross each other at $p^* = 0.19$. This behavior is incompatible with the conventional QCP scenario (Fig. 1(a)) [2, 3]. Instead, our results favor the RVB scenario (Fig. 1(b)). In the QCP scenario, T^* represents the temperatures of the phase transition [2, 3], whereas in the RVB model, $T_D(T_D^{(0)})$ represents crossover temperatures from the strange metal to the pseudogap (spin gap, to be precise) states [4–6]. In recent years, several phase transitions with symmetry breaking have been observed using vari-

ous techniques in the pseudogap regime [41–50], which may support the QCP scenario. We encountered a serious problem on reconciling these observations with our results, which is currently an open question. In this regard, Hussey argued that such phase transitions do not form a pseudogap, but instead involve the development of electronic instability inside the pseudogap regime [51]. Tallon and Loram argued that the pseudogap reflects an underlying energy scale E_g that vanishes beneath the superconducting dome [16]. The energy scale may correspond to the superexchange energy, J , and provide the crossover temperatures. Thus, we assumed that $T_{\rho_c}^*$ corresponds to $T_D^{(0)}$ of the RVB model [4–6].

The “strong” pseudogap effect has been predicted using the theories based on the Fermi-liquid point of view, which considers the effect of large antiferromagnetic spin fluctuations in quasi-two-dimensional metals near the Mott insulator [52–54]. In the RVB model, the “strong” pseudogap effect may be attributed to spinon pairing below T_D [4–6]. Furthermore, T_{coh} may correspond to the temperatures for Bose condensation of holons, T_{BE} , in the RVB model [6]. In this model, T_{BE} is proportional to the superfluid density $\rho_s(0)$. Our result of almost doping-independent T_{coh} in the overdoped region agrees with the experimental observation for $\rho_s(0)$ [55]. Consequently, our observed phase diagram (Fig. 5) roughly coincides with the prediction of the RVB model (Fig. 1(b)).

It is intriguing to note that this normal state crossing phenomena of $T_{\rho_c}^*$ and T_{coh} influences the nature of superconducting fluctuations. When $T_{\rho_c}^* < T_{coh}$ for $p > 0.19$, the phase ordering of Cooper pairs starts to develop almost simultaneously as they form below $T^{**} \approx T_{scf}$. When $T_{\rho_c}^* > T_{coh}$ for $p < 0.19$, Cooper pairs are preformed below T^{**} , but their phases are not settled. Thus, superconducting fluctuation does not appear until lower values of T_{scf} . This non-superconducting behavior between T_{scf} and T^{**} when $p < 0.19$ is consistent with the spinon pairing in the RVB model [4–6]. In addition, with decreasing p below 0.19, $T_{\rho_c}^*$ and T_c increase. This result implies that the pseudogap does not simply compete with superconductivity, but reflects the energy scale, J , which is probably the source for superconductivity.

Although our data are incompatible with the conventional QCP scenario, $p^* = 0.19$ may be an anomalous critical point. In this study, we found that $T_{\rho_c}^*$ and T_{coh} cross at p^* , and the preformed nature for Cooper pairing changes across this doping level. Therefore, $p^* = 0.19$ is closely related to superconductivity, and may be universal for hole-doped cuprates [16, 51]. This anomalous criticality at p^* was first proposed by Tallon and Loram [40].

Here, we assumed Eq. (1) and the incoherent to coherent crossover at $T_{coh} \approx 200$ K to interpret the temperature dependence of $\rho_{ab}(T)$. Alternatively, the power law formula may also reproduce the observed $\rho_{ab}(T)$ [56]. Another interpretation may be the achievement of the quantum mechanical constraint for the maximum scattering rate (Planckian dissipation limit) [13, 51, 57].

Summary.—In this study, we clarified the true phase diagram for the overdoped side of high- T_c cuprates. The frequently

discussed critical doping, $p^{**} = 0.19$, is a doping level above which T_{coh} can be observed clearly, and T^{**} approaches T_{scf} rapidly. These results agree with the RVB scenario, rather than the conventional QCP scenario, however an anomalous QCP scenario can not be ruled out. To complete the phase diagram, our approach must be extended to the underdoped side.

Acknowledgements.—The authors would like to acknowledge useful discussions with Y. Koike, T. Kondo, T. Shibauchi, and M. Ogata. This work was supported by a Hirosaki University Grant for Distinguished Researchers FY2017-2018. The magnetotransport measurements were performed using PPMS at Iwate University, the Institute for Solid State Physics, University of Tokyo, and Cryogenic Research Center, University of Tokyo. This work was supported by JSPS KAKENHI Grant Number 20K03849.

* twatana@hirosaki-u.ac.jp

- [1] M. R. Norman, D. Pines, and C. Kallin, *Adv. Phys.* **54**, 61 (2005).
- [2] C. M. Varma, *Phys. Rev. Lett.* **83**, 3538 (1999).
- [3] S. Sachdev, *Phys. Status Solidi B* **247**, 537 (2010).
- [4] P. A. Lee, N. Nagaosa, and X. G. Wen, *Rev. Mod. Phys.* **78**, 17 (2006).
- [5] M. Ogata and H. Fukuyama, *Rep. Prog. Phys.* **71**, 036501 (2008).
- [6] P. A. Lee and N. Nagaosa, *Phys. Rev. B* **46**, 5621 (1992).
- [7] B. Keimer, S. A. Kivelson, M. R. Norman, S. Uchida, and J. Zaanen, *Nature* **518**, 179 (2015).
- [8] T. Timusk and B. W. Statt, *Rep. Prog. Phys.* **62**, 61 (1999).
- [9] S. Hüfner, M. A. Hossain, A. Damascelli, and G. A. Sawatzky, *Rep. Prog. Phys.* **71**, 715 (2008).
- [10] A. A. Kordyuk, *Low Temp. Phys.* **41**, 319 (2015).
- [11] I. M. Vishik, *Rep. Prog. Phys.* **81**, 062501 (2018).
- [12] A. Kaminski, S. Rosenkranz, H. M. Fretwell, Z. Z. Li, H. Raffy, M. Randeria, M. R. Norman, and J. C. Campuzano, *Phys. Rev. Lett.* **90**, 207003 (2003).
- [13] N. E. Hussey, R. A. Cooper, X. Xu, Y. Wang, I. Mouzopoulou, B. Vignolle, and C. Proust, *Phil. Trans. R. Soc. A* **369**, 1626 (2011).
- [14] N. E. Hussey, H. Gordon-Moys, J. Kokalj, and R. H. McKenzie, *Journal of Physics: Conference Series* **449**, 012004 (2013).
- [15] U. Chatterjee, D. Ai, J. Zhao, S. Rosenkranz, A. Kaminski, H. Raffy, Z. Li, K. Kadowaki, M. Randeria, M. R. Norman, and J. C. Campuzano, *PNAS* **108**, 9346 (2011).
- [16] J. L. Tallon, J. G. Storey, J. R. Cooper, and J. W. Loram, *Phys. Rev. B* **101**, 174512 (2020).
- [17] S.-D. Chen, M. Hashimoto, Y. He, D. Song, K.-J. Xu, J.-F. He, T. P. Devereaux, H. Eisaki, D.-H. Lu, J. Zaanen, and Z.-X. Shen, *Science* **366**, 1099 (2019).
- [18] T. Usui, D. Fujiwara, S. Adachi, H. Kudo, K. Murata, H. Kushibiki, T. Watanabe, K. Kudo, T. Nishizaki, N. Kobayashi, S. Kimura, K. Yamada, T. Naito, T. Noji, and Y. Koike, *J. Phys. Soc. Jpn.* **83**, 064713 (2014).
- [19] Supplemental Materials at [URL] for annealing conditions and estimation of T_{scf} .
- [20] S. D. Obertelli, J. R. Cooper, and J. L. Tallon, *Phys. Rev. B* **46**, 14928 (1992).
- [21] T. Watanabe, T. Fujii, and A. Matsuda, *Phys. Rev. Lett.* **79**, 2113 (1997).
- [22] R. A. Cooper, Y. Wang, B. Vignolle, O. J. Lipscombe, S. M. Hayden, Y. Tanabe, T. Adachi, Y. Koike, M. Nohara, H. Takagi, C. Proust, and N. E. Hussey, *Science* **323**, 603 (2009).
- [23] A. Kaminski, S. Rosenkranz, H. M. Fretwell, M. R. Norman, M. Randeria, J. C. Campuzano, J.-M. Park, Z. Z. Li, and H. Raffy, *Phys. Rev. B* **73**, 174511 (2006).
- [24] S. Benhabib, A. Sacuto, M. Civelli, I. Paul, M. Cazayous, Y. Gallais, M.-A. Measson, R. D. Zhong, J. Schneeloch, G. D. Gu, D. Colson, and A. Forget, *Phys. Rev. Lett.* **114**, 147001 (2015).
- [25] K. Kadowaki and S. B. Woods, *Solid State Communications* **58**, 507 (1986).
- [26] N. E. Hussey, *J. Phys. Soc. Jpn.* **74**, 1107 (2005).
- [27] T. Watanabe, T. Fujii, and A. Matsuda, *Phys. Rev. Lett.* **84**, 5848 (2000).
- [28] K. K. Gomes, A. N. Pasupathy, A. Pushp, S. Ono, Y. Ando, and A. Yazdani, *Nature* **447**, 569 (2007).
- [29] K. Katsumi, Z. Z. Li, H. Raffy, Y. Gallais, and R. Shimano, *Phys. Rev. B* **102**, 054510 (2020).
- [30] T. Kondo, A. D. Palczewski, Y. Hamaya, T. Takeuchi, J. S. Wen, Z. J. Xu, G. Gu, and A. Kaminski, *Phys. Rev. Lett.* **111**, 157003 (2013).
- [31] T. J. Reber, N. C. Plumb, Z. Sun, Y. Cao, Q. Wang, K. McElroy, H. Iwasawa, M. Arita, J. S. Wen, Z. J. Xu, G. Gu, Y. Yoshida, H. Eisaki, Y. Aiura, and D. S. Dessau, *Nat. Phys.* **8**, 606 (2012).
- [32] T. J. Reber, N. C. Plumb, Y. Cao, Z. Sun, Q. Wang, K. McElroy, H. Iwasawa, M. Arita, J. S. Wen, Z. J. Xu, G. Gu, Y. Yoshida, H. Eisaki, Y. Aiura, and D. S. Dessau, *Phys. Rev. B* **87**, 060506(R) (2013).
- [33] T. Kondo, Y. Hamaya, A. D. Palczewski, T. Takeuchi, J. S. Wen, Z. J. Xu, G. Gu, J. Schmalian, and A. Kaminski, *Nat. Phys.* **7**, 21 (2011).
- [34] T. Kondo, W. Malaeb, Y. Ishida, T. Sasagawa, H. Sakamoto, T. Takeuchi, T. Tohyama, and S. Shin, *Nat. Commun.* **6**, 7699 (2015).
- [35] A. Dubroka, M. Rössle, K. W. Kim, V. K. Malik, D. Munzar, D. N. Basov, A. A. Schafgans, S. J. Moon, C. T. Lin, D. Haug, V. Hinkov, B. Keimer, T. Wolf, J. G. Storey, J. L. Tallon, and C. Bernhard, *Phys. Rev. Lett.* **106**, 047006 (2011).
- [36] E. Uykur, K. Tanaka, T. Masui, S. Miyasaka, and S. Tajima, *Phys. Rev. Lett.* **112**, 127003 (2014).
- [37] K. Lee, K. Kamiya, M. Nakajima, S. Miyasaka, and S. Tajima, *J. Phys. Soc. Jpn.* **86**, 023701 (2017).
- [38] Y. Wang, L. Li, and N. P. Ong, *Phys. Rev. B* **73**, 024510 (2006).
- [39] L. Li, Y. Wang, S. Komiya, S. Ono, Y. Ando, G. D. Gu, and N. P. Ong, *Phys. Rev. B* **81**, 054510 (2010).
- [40] J. L. Tallon and J. W. Loram, *Physica C* **349**, 53 (2001).
- [41] J. M. Tranquada, B. J. Sternlieb, J. D. Axe, Y. Nakamura, and S. Uchida, *Nature* **375**, 561 (1995).
- [42] G. Ghiringhelli, M. L. Tacon, M. Minola, S. Blanco-Canosa, C. Mazzoli, N. B. Brookes, G. M. D. Luca, A. Frano, D. G. Hawthorn, F. He, T. Loew, M. M. Sala, D. C. Peets, M. Saluzzo, E. Schierle, R. Sutarto, G. A. Sawatzky, E. Weschke, B. Keimer, and L. Braicovich, *Science* **337**, 821 (2012).
- [43] T. Hanaguri, C. Lupien, Y. Kohsaka, D.-H. Lee, M. Azuma, M. Takano, H. Takagi, and J. C. Davis, *Nature* **430**, 1001 (2004).
- [44] B. Fauqué, Y. Sidis, V. Hinkov, S. Pailhès, C. T. Lin, X. Chaud, and P. Bourges, *Phys. Rev. Lett.* **96**, 197001 (2006).
- [45] J. Xia, E. Schemm, G. Deutscher, S. A. Kivelson, D. A. Bonn, W. N. Hardy, R. Liang, W. Siemons, G. Koster, M. M. Fejer, and A. Kapitulnik, *Phys. Rev. Lett.* **100**, 127002 (2008).
- [46] M. Hashimoto, R.-H. He, K. Tanaka, J.-P. Testaud, W. Meevasana, R. G. Moore, D. Lu, H. Yao, Y. Yoshida, H. Eisaki,

- T. P. Devereaux, Z. Hussain, and Z.-X. Shen, *Nat. Phys.* **6**, 414 (2010).
- [47] Y. Ando, K. Segawa, S. Komiya, and A. N. Lavrov, *Phys. Rev. Lett.* **88**, 137005 (2002).
- [48] R. Daou, J. Chang, D. LeBoeuf, O. Cyr-Choinière, F. Laliberté, N. Doiron-Leyraud, B. J. Ramshaw, R. Liang, D. A. Bonn, W. N. Hardy, and L. Taillefer, *Nature* **463**, 519 (2010).
- [49] K. Ishida, S. Hosoi, Y. Teramoto, T. Usui, Y. Mizukami, K. Itaka, Y. Matsuda, T. Watanabe, and T. Shibauchi, *J. Phys. Soc. Jpn.* **89**, 064707 (2020).
- [50] Y. Sato, S. Kasahara, H. Murayama, Y. Kasahara, E.-G. Moon, T. Nishizaki, T. Loew, J. Porras, B. Keimer, T. Shibauchi, and Y. Matsuda, *Nat. Phys.* **13**, 1074 (2018).
- [51] N. E. Hussey, J. Buhot, and S. Licciardello, *Rep. Prog. Phys.* **81**, 052501 (2018).
- [52] A. Kobayashi, A. Tsuruta, T. Matsuura, and Y. Kuroda, *J. Phys. Soc. Jpn.* **70**, 1214 (2001).
- [53] Y. Yanase and K. Yamada, *J. Phys. Soc. Jpn.* **70**, 1659 (2001).
- [54] S. Onoda and M. Imada, *J. Phys. Soc. Jpn.* **69**, 312 (2000).
- [55] J. L. Tallon, J. W. Loram, J. R. Cooper, C. Panagopoulos, and C. Bernhard, *Phys. Rev. B* **68**, 180501(R) (2003).
- [56] T. J. Reber, X. Zhou, N. C. Plumb, S. Parham, J. A. Waugh, Y. Cao, Z. Sun, H. Li, Q. Wang, J. S. Wen, Z. J. Xu, G. Gu, Y. Yoshida, H. Eisaki, G. B. Arnold, and D. S. Dessau, *Nat. Commun.* **10**, 5737 (2019).
- [57] J. Zaanen, *Nature* **430**, 512 (2004).

Revised phase diagram of a high- T_c cuprate superconductor revealed by anisotropic transport measurements

Keiichi Harada,¹ Yuki Teramoto,¹ Tomohiro Usui,¹ Kenji Itaka,² Takenori Fujii,³ Takashi Noji,⁴ Haruka Taniguchi,⁵ Michiaki Matsukawa,⁵ Hajime Ishikawa,⁶ Koichi Kindo,⁶ Daniel S. Dessau,⁷ and Takao Watanabe^{1,*}

¹Graduate School of Science and Technology, Hirosaki University, Hirosaki, Aomori, 036-8561 Japan

²Institute of Regional Innovation, Hirosaki University, Aomori, Aomori, 036-8561 Japan

³Cryogenic Research Center, University of Tokyo, Bunkyo, Tokyo 113-0032, Japan

⁴Graduate School of Engineering, Tohoku University, Sendai 980-8579, Japan

⁵Graduate School of Engineering, Iwate University, Morioka 020-8551, Japan

⁶Institute for Solid State Physics, University of Tokyo, Kashiwa, Chiba 277-8581, Japan

⁷Department of Physics, University of Colorado at Boulder, Boulder, CO 80309, USA

(Dated: February 28, 2022)

A. SAMPLE PREPARATION

To control the doping level (p), single crystals were annealed under the conditions listed in Table I. After annealing, they were rapidly cooled to room temperature at a rate of approximately 30 °C/min under the same conditions.

B. ESTIMATION OF THE ONSET OF SUPERCONDUCTING FLUCTUATION (T_{scf})

To investigate the relationship between the “weak” and “strong” pseudogap opening temperatures and T_{scf} , T_{scf} was estimated by comparing the values of $\rho_{ab}(T)$ with and without a magnetic field. The plots of the temperature derivative of $\rho_{ab}(T)$ with and without a magnetic field of 9 T as a function of the temperature for different doping levels are depicted in Fig. 1(a), 1(b), 1(c), and 1(d). Here, T_{scf} is defined as the temperature at which $d\rho_{ab}(T)/dT$ under a magnetic field of 9 T decreases by 1 %, relative to that without a magnetic field. This definition is based on the fact that a positive magnetoresistance appears below T_{scf} due to the suppression of the Aslamazov–Larkin type superconducting fluctuation effect [1]. Consequently, T_{scf} is estimated as 119, 113, 97, and

86 K for $p = 0.179, 0.194, 0.206$, and 0.220 , respectively. T_{scf} for $p = 0.232$ was previously estimated as 73 K [1].

* twatana@hirosaki-u.ac.jp

[1] T. Usui, D. Fujiwara, S. Adachi, H. Kudo, K. Murata, H. Kushibiki, T. Watanabe, K. Kudo, T. Nishizaki, N. Kobayashi, S. Kimura, K. Yamada, T. Naito, T. Noji, and Y. Koike, J. Phys. Soc. Jpn. **83**, 064713 (2014).

TABLE I. Summary of annealing conditions, T_c , and their doping levels (p) used in the in-plane resistivity measurements. The same conditions were used for the out-of-plane resistivity measurements, except for slight changes in T_c and p .

Annealing Conditions	T_c	p
600 °C, 24 h in O ₂ 2 Pa	89.6 K	0.177
600 °C, 12 h in O ₂ 10 Pa	87.0 K	0.185
600 °C, 12 h in O ₂ 100 Pa	84.5 K	0.191
600 °C, 18 h in O ₂ 1 %	79.0 K	0.201
600 °C, 18 h in O ₂ 10 %	75.0 K	0.207
600 °C, 36 h in O ₂ 100 %	70.7 K	0.213
500 °C, 70 h in O ₂ 100 %	67.4 K	0.217
400 °C, 200 h in O ₂ 100 %	65.1 K	0.219
400 °C, 200 h in O ₂ 100 % 420 atm	56.3 K	0.228
400 °C, 30 h in O ₂ 100 % 400 atm (pristine)	52.0 K	0.232

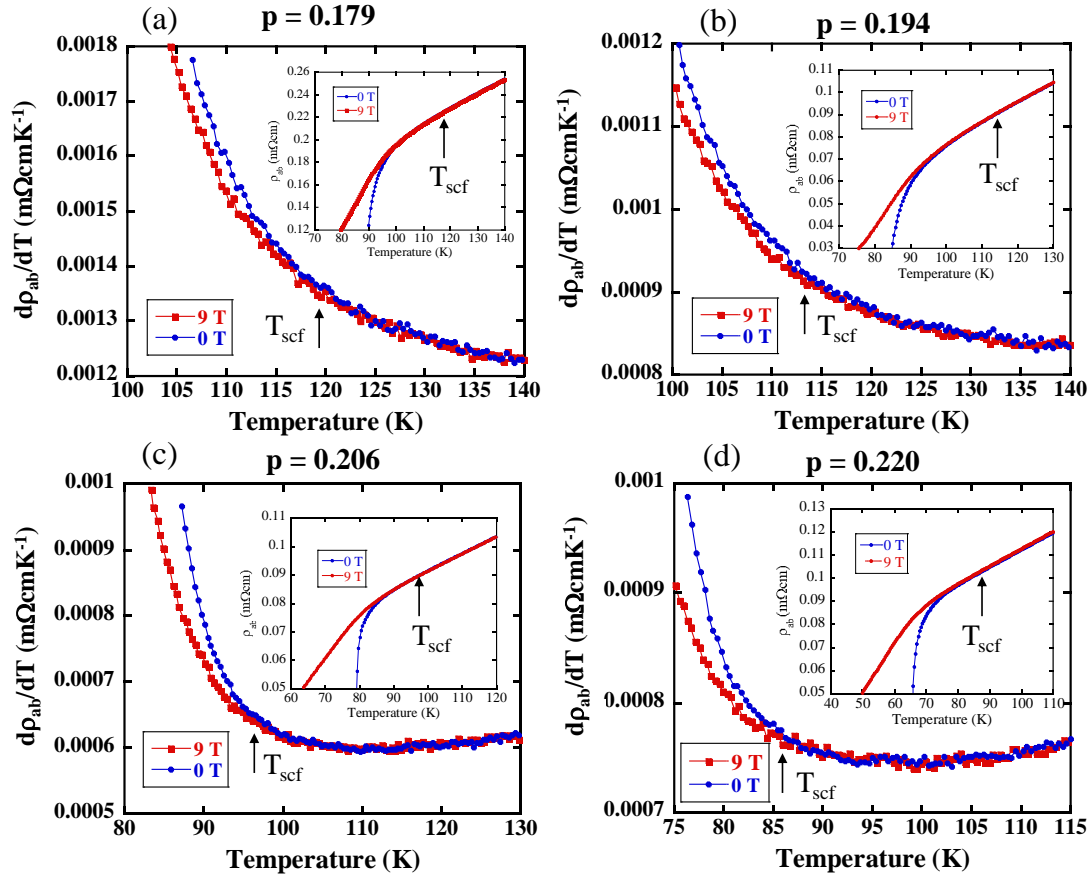


FIG. 1. (Color online) Temperature derivative of ρ_{ab} vs. the temperatures with and without a magnetic field of 9 T for (a) $p = 0.179$, (b) $p = 0.194$, (c) $p = 0.206$, and (d) $p = 0.220$. The temperatures T_{scf} below which $d\rho_{ab}/dT$ with a magnetic field of 9 T deviates from that without a magnetic field are indicated by arrows. The inset shows ρ_{ab} vs. temperatures with and without a magnetic field of 9 T.